Toxicant production in under-ventilated compartment fires assessed by laser absorption spectroscopy

Rayna Vreeland[a], Kyle L. Fetter[b], Nicolas S. B. Jaeger[c], Yi Yan[c], Xiuqi Xi[a], James L. Urban[a,*], Daniel I. Pineda[b] and R. Mitchell Spearrin[c]

[a]Department of Fire Protection Engineering, Worcester Polytechnic Institute (WPI), 100 Institute Rd., Worcester, 01609, MA, USA
[b]Department of Mechanical, Aerospace, and Industrial Engineering, UT San Antonio, 1 UTSA Circle, San Antonio, 78249, TX, USA
[c]Department of Mechanical and Aerospace Engineering, UC Los Angeles, 420 Westwood Plaza, Los Angeles, 90095, CA, USA

ARTICLE INFO

Keywords:
fire toxicity
laser absorption spectroscopy
compartment fire
emission factor

ABSTRACT

The production of incomplete combustion products from the burning of wood, medium density fiberboard (MDF), and nylon in an under-ventilated compartment fire was investigated using a reduced-scale compartment. Species measurements of carbon monoxide (CO) and carbon dioxide (CO_2) were performed using Fourier Transform Infrared Spectroscopy (FTIR) and methane (CH_4), hydrogen cyanide (HCN), benzene (C_6H_6), ethylene (C_2H_4) and acetylene (C_2H_2) were measured with Laser Absorption Spectroscopy (LAS) with three different interband cascade lasers. The fuels were burned in three different crib configurations; only wood, only MDF, and a mixture of wood and nylon, to examine the production of different toxicants. During the experiments, measurements were collected of CO, CO_2, CH_4, HCN, C_2H_2, and C_6H_6 species from the gas exiting the compartment, gas temperature from inside the compartment, and the flow into and out of the compartment. Consistent with under-ventilated combustion, the temperature inside the compartment typically exceeded 600°C. CO was measured during all experiments and was two orders of magnitude less than the measured CO_2 concentration. Significant amounts of unburned hydrocarbons were measured during all of the experiments, while HCN was only detected during the wood-nylon tests. Higher toxicant yields were measured for wood-nylon compared to pure wood and MDF.

1. Introduction

During structure fires, toxic gas species are produced, and these are responsible for the majority of fire related deaths, posing significant health hazards to firefighters [1]. Firefighters are continuously exposed to toxic gases when they are fighting fires, via inhalation of contaminated air or absorption through the skin. Recent studies have shown that exposure to toxic gases is not completely eliminated when firefighters use self-contained breathing apparatus (SCBA) [2, 3]. Volatile organic compounds, including benzene, can penetrate through firefighters' personal protective equipment (PPE), allowing for transdermal absorption. To understand exposure risk and potential impact on firefighter health, it is important to characterize the ambient conditions to which firefighters, and their PPE, are exposed.

The amount and rate of production of toxic gas species depends on the amount of oxygen available during combustion as well as on the chemical composition of the fuels burned [4]. Generally, in under-ventilated fires where oxygen is limited, more incomplete combustion products are produced, such as carbon monoxide (CO), hydrogen cyanide (HCN), and unburned hydrocarbons (UHC) [5]. In contrast, a well-ventilated fire occurs when ample oxygen is present compared to the amount of fuel burned, and thus typically exhibits more complete combustion with less toxic gas species produced. The health impacts of toxic gas species can be immediate or long term; exposure to asphyxiant gases such as CO and HCN can result in incapacitation, even death, depending on the dose [6]. On the other hand, exposure to benzene has been associated with elevated cancer risk [1]. Additionally, UHC and CO also present a risk of contributing toward a flammable atmosphere allowing for the possibility of backdraft or explosions depending on the conditions. To fully assess the toxicity of gases contaminated by the combustion products of under-ventilated compartment fires, it is important to characterize as many of the high impact species as possible, because the health effects of these species are additive [1]. In post-fire scenarios and firefighter operations such as overhaul, firefighters may be working in a room with lingering combustion products from the extinguished fire and combustion products from so-called "hidden fires" in the walls that may smolder or burn with underventilated conditions. In these scenarios, the combustion products may have mixed well with air. In some cases, this could create a situation of ambiguous tenability which cannot be assessed without the aid of a suitable gas sensor.

Species measurements during under-ventilated combustion have been investigated since the 1970s [7]. Studies have primarily focused on characterizing the yields of select species, including CO, carbon dioxide (CO_2), nitrogen oxides, HCN, and UHC, for many different fuels, while varying the equivalence ratio. These measurements have been conducted at varying scales from small-scale benchtop apparatuses, such as the steady-state tube furnace or the fire

*Corresponding author
rlvreeland@wpi.edu (Rayna Vreeland); kyle.fetter@my.utsa.edu (Kyle L. Fetter); jaeger4@g.ucla.edu (Nicolas S. B. Jaeger); yydjx@ucla.edu (Yi Yan); xixiuqi@outlook.com (Xiuqi Xi); jurban@wpi.edu (James L. Urban); daniel.pineda@utsa.edu (Daniel I. Pineda); spearrin@ucla.edu (R. Mitchell Spearrin)
ORCID(s):

propagation apparatus (FPA) [5, 8–10], to compartment fire experiments [8, 11–13].

In these studies, researchers have used a variety of different species measurement techniques, including: Fourier Transform Infrared Spectrometer (FTIR) [8, 9, 11], electrochemical sensors [14], and gas absorption methods [11]. FTIR is an absorption-based method often operated with a continuous gas sampling flow, wherein broadband spectrally-resolved scans of the gas are collected at regular time intervals (often spanning ∼10 s to several minutes) and with spectral resolutions on the order of 0.125–16 cm^{-1} [9, 11]. There is a trade-off between time resolution and spectral resolution, and so in dynamic fire environments, a sampling interval of 10 s and moderate spectral resolution of 4 cm^{-1} is often employed to best capture an evolving gas composition produced by a fire. An advantage of FTIR over other measurement techniques is that it can be used to measure a multitude of species at once using only one device, but the number and kind of species that can be measured are limited by the operation resolution. At a resolution of 4 cm^{-1}, which was used by [9, 11], some species can be missed due to interference of water or other prominent species in combustion, exacerbated by relatively poor sensitivity associated with difficulties enhancing optical pathlength with broadband light ($\geq$ 1 cm^{-1}) [15]. At higher spectral resolutions, the scan duration increases, limiting the ability to achieve time-resolved measurements and possibly requiring bagged samples to be taken and analysis conducted post-test. FTIR measurements typically require multi-point calibrations for each species, and the accuracy of the measurements depends on maintaining control of the temperature and pressure, making it difficult to achieve accurate results in dynamic environments [16]. Unlike FTIR, electrochemical sensors require unique devices for each measured species, although selectivity can be challenging. Electrochemical sensors can be inexpensive, simple to deploy, and can provide time-resolved measurements, but they require frequent calibration, are sensitive to adverse conditions, and can have trouble with interfering species [17]. Sorbent tube measurements are also frequently employed, but these techniques cannot provide time-resolved measurements, as they rely on measurements of samples collected over extend time periods. Thus, to better characterize the dynamic gas-phase thermochemistry in compartment fires—which can offer faster and less expensive experimental turnaround but accordingly exhibit shorter-lived behavior—high-time resolution measurements are needed that can quantify the dynamically evolving species concentrations.

The measurement techniques discussed above exhibit many technical limitations that have motivated the development of the laser absorption spectroscopy (LAS) sensors presented in this work. LAS systems measure the attenuation of laser light at a strategically chosen wavelength that targets narrow-band features of a molecule's unique spectral absorption fingerprint to derive measurements of gas concentration and thermodynamic properties [18]. The governing equation for LAS sensors is the Beer-Lambert Law,

$$\alpha(\nu) = -\ln\left(\frac{I_T(\nu)}{I_0(\nu)}\right), \tag{1}$$

where $\alpha(\nu)$ is spectral absorbance and $I_T(\nu)$ and $I_0(\nu)$ are the spectral transmitted and background intensities of light, respectively [18]. The expression for spectral absorbance can also be related to gas properties as follows,

$$\begin{aligned}\alpha(\nu) &= \sum_i X_i S_j(T)\phi_i(\nu, T, P, X_i)PL \\ &= \sum_i X_i n_i \sigma_i(\nu, T, P)L\,,\end{aligned} \tag{2}$$

where X_i is the mole fraction of species, i, S_j is the linestrength of spectral line j, ϕ is lineshape, P is pressure, L is pathlength, n is species number density, and σ is absorbance cross section [18].

Strategic wavelength selection allows LAS systems to be highly species specific. This represents a major advantage over electro-chemical sensing options, which are often cross-sensitive to many species other than those for which it is intended to measure [19]. Advancements in precision, high-speed electronics allow LAS systems to achieve comparable measurement quality to the most precise, lab-grade techniques (such as FTIR) with a much higher temporal resolution. For highly dynamic systems, such as fires, high temporal resolution is necessary to better understand the progression of effluent toxicity over the course of the fire's development. The required electronics are also very compact, allowing LAS systems to be portable and used in-situ. Furthermore, scanned-wavelength LAS sensors provide a ratiometric measurement that has been shown to be both calibration-free and impervious to biasing due to scattering, beam-steering, and fouling [20–22]. These attributes have been shown to be resilient to smoke-induced sensor fouling in large-scale fire experiments [23].

This study seeks to understand the production of selected chemical species from the under-ventilated combustion of fuel cribs composed of: wood, medium-density fiberboard (MDF), and a mixture of nylon with wood; and to demonstrate the use of novel sensing technologies (LAS) for collecting time-resolved species measurements. The selected chemical species are: CO, CO_2, methane (CH_4), acetylene (C_2H_2), benzene (C_6H_6), ethylene (C_2H_4), and HCN. This includes a selection of toxicant gases, which may pose a risk to tenability in fires [1]. The production of these species is quantified in terms of the species concentration in the exhaust stream and yields for the fuel packages during under-ventilated burning conditions. The species concentrations are obtained using a combination of Fourier Transform infrared spectroscopy and advanced scanned-wavelength LAS sensors that were purpose built for measurements of fire effluents. With flow measurements, the yields of these species are calculated.

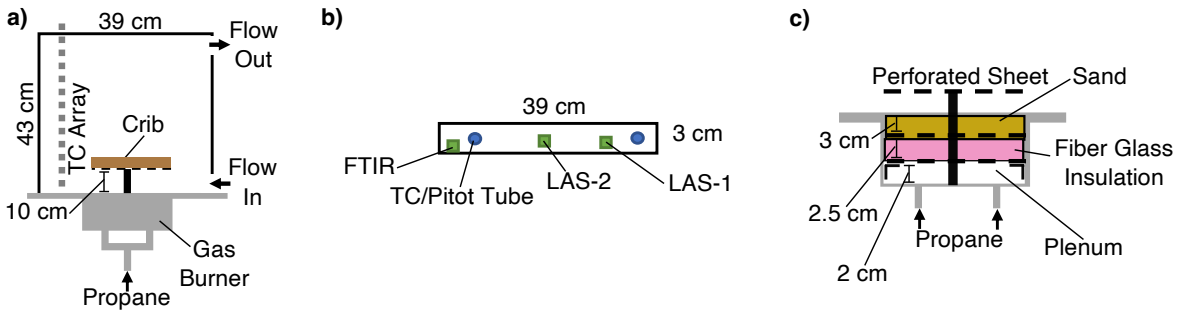

Figure 1: Schematic of the experimental setup: a) Side view, b) Front view of upper slit with sensor measurement locations, c) Detailed view of internal components of the gas burner configuration. The gas species that were measured at each sampling location were: CO and CO_2 for the FTIR; C_6H_6 and C_2H_4 for LAS-1; and C_2H_2, CH_4, and HCN for LAS-2.

2. Experimental Methods

To analyze the toxic gas production from under-ventilated compartment fires, fuel crib packages were burned inside an insulated compartment with internal dimensions: 39 cm × 39 cm × 43 cm , (Fig. 1a). The compartment was constructed in two pieces: a floor-mounted gas burner and a box providing the walls and ceiling of the compartment. The box was built from 3.4 mm-thick sheets welded together with two removable inner layers of 1.6 cm-thick drywall (fire code USG Sheetrock) for insulation. Each side except the front was fabricated from solid A1011 hot-rolled steel sheets. The steel front wall spanned the full width, but did not connect to the top and bottom of the box. The drywall inserts extended further vertically, leaving two 39 cm wide by 3 cm tall slits (see Fig. 1a & b). This two-slit configuration for the ventilation of the compartment was used based on the ventilation design used by Utiskul et al. [24]. This ventilation configuration was chosen, because it facilitates characterization of the mass flows in and out of the compartment.

The floor-mounted gas burner included a 0.34 cm thick 50 cm by 50 cm steel plate with a centered 25 cm by 25 cm gas burner. Propane entered at the bottom of the burner through two openings into the plenum in the burner (see Fig. 1c). A plenum and two porous layers produce a uniform mass flux of propane from the burner. The first porous layer is a 2.54 cm layer of fiber glass insulation between two perforated sheets. The remaining depth of the burner (~3 cm) was filled with sand.

A table was used to hold the crib. It was built with a 25 cm by 25 cm perforated steel sheet top 10 cm above the compartment floor and was supported by a single 3.2 cm diameter post centered in the gas burner. A layer of ceramic fiber blanket was used as a gasket between the two compartment pieces to minimize leakage.

During the experiments, fuel cribs were placed on the table inside the compartment. The cribs were built from 25 cm-long sticks with a 1.9 cm-square cross section arranged in three layers with five sticks per layer (Fig. 2). The composition of the cribs varied between experiments to examine the production of different toxicants. Three different crib compositions were tested: all wood sticks, all medium density fiberboard (MDF) sticks, and a combination of 10 wood sticks and 5 nylon sticks making up the top layer of the crib. The wood sticks were listed by the supplier as mixture of spruce, pine, and fir. The sticks were stored in an air-conditioned room for at least 1 week prior to the experiments. The sticks were attached using brad nails for wood and MDF and using J-B Weld Epoxy adhesive for nylon to form the cribs.

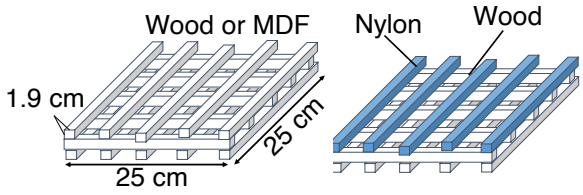

Figure 2: Schematic of crib configurations *Left:* Single-fuel crib (wood or MDF), *Right:* Dual-fuel crib (wood and nylon).

The goal of this study is to analyze the toxic gas species produced from these fuel cribs, so the gas burner was only used for the first 90 s of the experiment to ignite the crib. To begin the test, the gas burner was ignited using a propane torch and 20 L/min of propane was supplied for the first 90 s. Each experiment continued until flaming combustion was no longer observed inside the compartment. The end of flaming combustion of the crib was visually observed through the lower slit from below. Once the fire compartment fire reached the decay phase, the lower slit was closely monitored to ensure that the test duration was consistent between experiments. A total of 19 experiments were conducted: 11 wood, 3 MDF, and 5 wood/nylon. Mass flow, temperature, and species transient measurements were collected during the experiments, but due to equipment failure or other constraints not all measurements were available during every experiment. The number of experiments where each measurement was successfully collected are summarized in Table 1.

The flow in and out of the compartment was characterized using two measurement locations at each slit opening. Each measurement location was located mid-height of the slit (~1.5 cm) with one located 10 cm from the left side of the slit and the other 5 cm from the right side of the

Table 1
Number of experiments where each measurement was successfully collected. Temperature measurements were successfully collected during every experiment.

Fuel	Mass Flow	CO/CO_2	C_6H_6 /C_2H_4	C_2H_2/CH_4 /HCN
Wood/ Nylon	5	4	1	2
MDF	3	2	1	1
Wood	10	4	1*	3

* Mass Flow measurements were not collected during this experiment

slit (Fig. 1b). It was assumed that the flow of each slit is spatially uniform, since the height of the slit is only 3 cm. For each flow measurement, a PerfectPrime PT6302 stainless steel s-type pitot tube (6 mm x 300 mm) and a 0.25 mm K-type thermocouple were co-located. The differential pressure measurements from the s-type pitot tubes were collected with Sensirion SDP800-125Pa pressure transducers at 20 Hz and the temperature measurements were collected at 1 Hz. The velocity of the flow was calculated using the Bernoulli equation [25], and with area of the vent, the mass flow rate of effluents out of the compartment can also be calculated.

$$u = k\sqrt{\frac{2\Delta P}{\rho}} \tag{3}$$

$$\dot{m}_{\text{out}}(t) = \rho\big(T(t)\big)\, u_{\text{out}}(t)\, A \tag{4}$$

where k is the probe coefficient for the s-type pitot tubes, ΔP is the differential pressure measurement, A is the area of the area of the upper slit, and ρ is the density of the gas calculated using the ideal gas law at the temperature (T) of the associated thermocouple measurement. This assumes that each slit vent, exhibits uniform one-way flow and that the flow out temperature and composition of the flow for each slit is independent of position [24].

Three gas sampling lines were placed at the top vent. Each sampling line led to one of the three gas sensors: the FTIR and the two LAS sensors (see Fig. 4 and Fig. 7). It is assumed that the gases exiting are well mixed with the same composition. A detailed description of these measurements is provided in the following section.

3. Emissions Measurements

3.1. CO and CO_2 Measurements with Fourier Transform Infrared Spectroscopy

The FTIR was used to measure carbon monoxide (CO) and carbon dioxide (CO_2) with a 2 m path length gas cell. The gas was continuously sampled at 2 L/min and filtered through a coarse soot filter and a United Filtration Systems 10 micron stainless steel filter (DIF-BN10SS). The sampling line length was minimized and the majority of the sampling line was insulated to prevent water condensation. Ambient air was used for the FTIR background intensity measurement of $I_0(\nu)$, collected before each experiment. Each collected spectra comprised 36 scans resulting in a measurement about every 30 s. These spectra were used to measure the concentration of CO and CO_2 by fitting the spectra to HITRAN spectral data from 2100–2225 cm^{-1} and 2200–2400 cm^{-1} respectively [26]. The relative uncertainty in the concentration measurements was 24% for CO and 23% for CO_2, (see Appendix A).

Figure 3 shows a representative sample of the collected concentration profiles for CO and CO_2. Significant amounts of CO were produced during every experiment, typical of under-ventilated fires. The measured peak CO concentration was highest for the wood/nylon crib and lowest for the pure wood crib. The variation in the measured concentration of CO_2 between the different fuels is less than that of CO, with the wood/nylon cribs and the MDF crib having a larger concentration of CO_2. The measured CO concentrations are two orders of magnitude less than the measured CO_2 concentration for all the fuels. The measured CO/CO_2 ratio is consistent with other small scale test results, where the majority of reported CO/CO_2 ratios are on the order of $\mathcal{O}(10^{-2})$ [27–30]. But the ratio is smaller than most under-ventilated large scale fire measurements, where the majority of the reported CO/CO_2 ratios are on the order of $\mathcal{O}(10^{-1})$ [27, 31].

3.2. C_6H_6 and C_2H_4 Measurements via Scanned-Wavelength Laser Absorption Spectroscopy

A tunable interband cascade laser (ICL) absorption spectroscopy sensor was developed primarily to measure benzene (C_6H_6) production from fire effluents. The sensor targets a C_6H_6 feature near 2006 cm^{-1} (4.98 μm) that is likely attributable to a summation band of the E_{2u} and B_{2g} out-of-plane C−H bending modes [32]. The selected feature is chosen for its relatively narrow spectral structure when compared to other absorption features that have been used for LAS sensing of C_6H_6 (typically targeting the C-H stretch around 3000–3300 cm^{-1} (3–3.3 μm)) [33, 34]. This allows for the differential absorption to be well-resolved by a narrow-band distributed feedback (DFB) ICL. The feature's absorptivity is also appropriate to measure relevant concentrations of C_6H_6—known to pose chronic health risk to humans—at a pathlength that is viable for a portable sensor [35]. A survey of the absorption profiles of other combustion relevant species (including CO, CO_2, H_2CO, CH_4, C_2H_2, NO, N_2O, HCN, and the other BTEX molecules, such as benzene, toluene, and ethylbenzene, and xylene) indicated that the absorption spectrum of the selected feature is sufficiently isolated from those of potentially interfering species to facilitate quality C_6H_6 measurements [26, 36]. The only concerning interfering species are ethylene (C_2H_4) and water (H_2O); however, they are distinct enough to be effectively accounted for, and measured, with a multi-spectral least-squares fitting algorithm [26, 37]. LAS sensors for C_2H_4 also typically target the C-H stretch around 3000–3300 cm^{-1} or its overtone around 6250 cm^{-1} (1.6 μm) [38, 39]. However, for this work it is advantageous to only use one laser and detector to measure both species of interest.

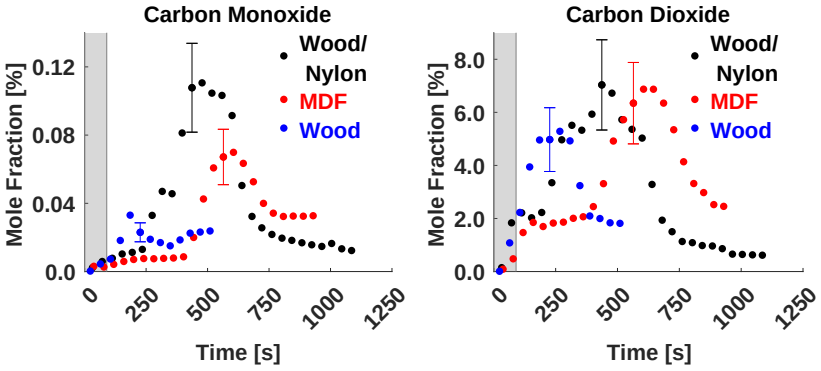

Figure 3: Mole fraction measurements of CO and CO_2 in time for the varying fuels. The the uncertainty in the concentration measurements are shown by the error bars. The grey shaded region indicates when the propane burner was on.

The optical sensor setup (shown in Fig. 4) uses a Nanoplus DFB ICL centered around 2006 cm^{-1} to access the chosen C_6H_6 feature. The output light intensity is measured with a VIGO Photonics PVI-4TE-5-1X1 photovoltaic detector. The sample gas is drawn through a Thorlabs HC10L-M02 Herriott cell, which achieves a 10.4 m pathlength in a 16.3" × 5.51" × 4.45" volume. The laser is controlled with an Arroyo Instruments 6305 Laser Diode Controller. The laser scan is controlled by the analog output function of a National Instruments PCI-6115 DAQ card (installed in a PXIe-1073 chassis) via the Arroyo controller. The NI board's analog input is also used to record and save the detector signal to a control laptop for subsequent post-processing.

Prior to each test, the sensor was purged with dry N_2 and a background measurement was performed. The sampling system was then switched to measure from the fire emissions sampling line. The spectral absorbance of the sample gas was calculated from the Beer-Lambert law using the raw fire data and the measured background as inputs. The laser was scanned sinusoidally at 1000 Hz and 1000-cycle averaging was applied, resulting in a measurement rate of 1 Hz. A representative one-second averaged scan showing C_6H_6, C_2H_4, and H_2O absorbance and simultaneous spectral fits obtained from a 2:1 wood/nylon crib fire is provided in Fig. 5. The C_6H_6 absorbance is derived from pressure-specific cross sections that were measured in a controlled gas cell and the C_2H_4 and H_2O absorbance spectra were fit with standard Voigt profiles [40]. The total fit is shown to be within 5% residual of the measured data across the spectral range of the laser scan. A conservative minimum detectable absorbance of 0.003 was used to define the detection limit for this study based on the baseline noise taken from a representative non-absorbing scan. The characteristic uncertainties for species mole fraction of C_6H_6 and C_2H_4 are range from approximately 5-9% and 20-30%, respectively, depending on the fuel load in a given test (see Appendix A). The uncertainty in each test varies depending on the amount of each species present. The C_2H_4 uncertainty is higher due to high linestrength uncertainty, which could be reduced with future validation measurements. The fitting algorithm was applied to each one-second averaged scan collected over the duration of the fires to develop emission time histories of target gases.

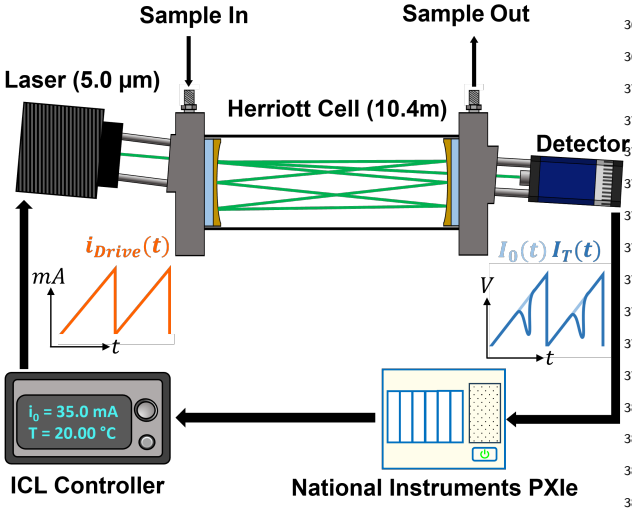

Figure 4: Schematic of the LAS sensors for C_6H_6.

The benzene and ethylene time histories for three of the crib materials are provided in Fig. 6. It is clear from these plots that the wood/nylon fuel load produces considerably higher emissions of C_6H_6 and C_2H_4 than the MDF and wood fuels. This is likely due, in part, to the tendency of wood and other cellulosic fuels to char, unlike nylon. Consequently for the wood tests, a smaller fraction of the fuel is gasified as combustion products or unburned hydrocarbons, like the species measured in this study. This difference in pyrolysis mechanisms may also partly explain why the peak emission duration time histories from the wood/nylon fires were longer than that of pure wood. Furthermore, the density of nylon is approximately 1.14 g/cm^3, larger than the value for wood, typically less than 1.0 g/cm^3, meaning there is more mass of fuel per crib [41, 42]. This likely also contributes to the differences in the observed emissions quantities and time scales. The peak concentrations of C_6H_6 and C_2H_4 are on the same order of magnitude for the wood and MDF tests. However, the emission production duration for MDF is similar to

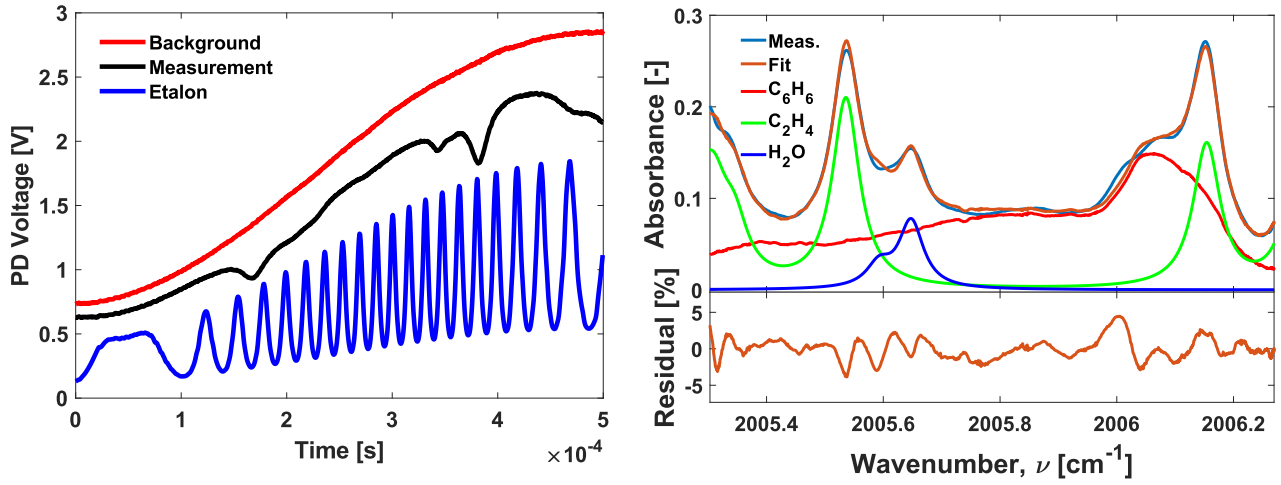

Figure 5: Raw photodetector measurement for a representative wood/nylon fire and etalon measurement, which is used to develop a relationship between relative wavenumber and time, (left) and the associated post-processed absorbance spectra near 2006 cm^{-1} (4.98 μm) showing the multi-spectral fit for benzene, water, and ethylene (right) [26, 37].

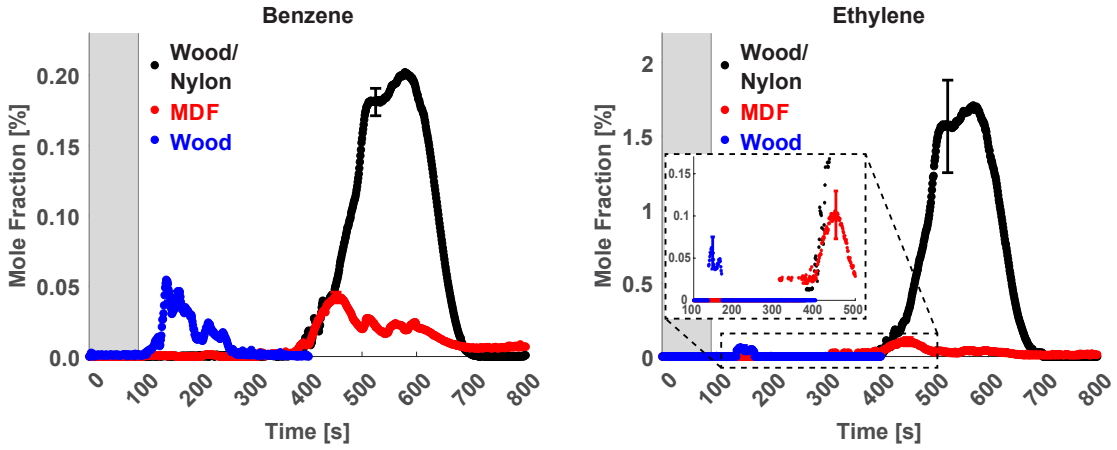

Figure 6: Mole fraction measurements for C_6H_6 and C_2H_4 in time for the varying fuels. The the uncertainty in the sensor is illustrated with a representative error bar for each species. The shaded region indicates when the time during which the propane burner was on.

that of the wood/nylon dataset, and is approximately twice that of the wood. This may also be attributed to different pyrolysis mechanisms associated with the composition of MDF. MDF typically consists of 82% wood fiber (cellulose), but also contains binding agents to hold the fibers together [43]. Standard MDF contains 9% urea-formaldehyde and 1% paraffin wax [42, 43]. As with the comparison between the wood and nylon, the binding agents likely do not form a char like the wood fibers do.

It is demonstrated in Fig. 6 that the C_2H_4 production is greater than that of C_6H_6 for all fuels. This aligns with the anticipated chemical pathway of thermal decomposition for organic matter in under-ventilated environments [44]. It should be noted that, in the case of wood, the C_2H_4 concentration is below the sensors limit of detection for large portions of the test. The limit of detection for C_2H_4 is much higher than that of C_6H_6 for this sensor because of its locally weaker linestrength.

3.3. C_2H_2, CH_4, and HCN Measurements via Wavelength Modulation Spectroscopy

A second sensor was designed to target C_2H_2, CH_4, and HCN and implemented in this experiment using wavelength modulation spectroscopy (WMS). WMS is an advanced tunable laser spectroscopy technique that uses the overtone frequency bands of a superimposed sinusoidal laser injection function allowing for signal intensity independence and increased noise filtering [45]. This method allows for the calibration-free technique of LAS to be further exploited and allow for reduction in signal due to smoke and other particulates common in under-ventilated fires [46].

The multi-pass optical sensor is similar to that described in prior work by the authors [47]. For this experiment, an optical setup shown in Fig. 7 uses two light sources: an ICL targeting one R-branch transition (R(2)) and three Q-branch transitions (Q(6)) near 2676 cm^{-1} (3.74 µm) of the $2\upsilon_4$ asymmetric stretch overtone band of CH_4, and an ICL near

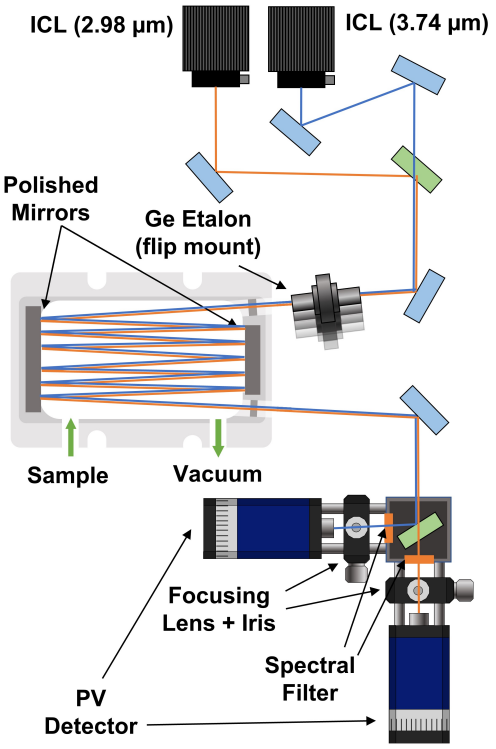

Figure 7: Scanned-WMS optical setup deployed for HCN, CH_4, and C_2H_2.

3352 cm^{-1} (2.98 µm) targeting the R(0,14) transition in the υ_1 asymmetric stretch band of HCN and R(0,25) and R(0,31) transitions of the υ_3 CH stretch and $\upsilon_2+\upsilon_4+\upsilon_5$ combination bands of C_2H_2. These species have been commonly probed using both LAS and WMS in fire environments [48, 49]. The line selection used in this study is ideal due to the low number of potential spectral interfering species (CO, CO_2, H_2O, NO and N_2O) for the selected fuel types and expected concentrations. Formaldehyde is the main interferer for the 3352 cm^{-1} (2.98 µm) light source and was considered as an additional measurement species, however was not detected above the estimated detection limit (100 ppm) throughout the testing campaign.

This sensor used a narrow bandpass spectral filter centered at the wavelength of each light source, beam splitters, a 2" germanium etalon and a 1-m pathlength multipass optical gas cell (Thorlabs MGC1C-P01) with polished stainless steel mirrors to allow for corrosion resistance and easy replacement due to mirror fouling. To more flexibly co-align the two different laser beams, an alternative pathlength was used through the cell, reducing the optical pathlength from the designed 1 m to $L = 0.625 \pm 0.050$ m (measured spectroscopically using barometrically controlled mixtures of C_2H_2). This reduction in pathlength decreased our ultimate emission sensitivity; however, it allowed for higher signal throughout testing after mirror fouling and smoke obfuscation occurred. The optical cell used a small air pump to sample the gas through the cell (1.7 s refresh time) with a coarse filter in the tubing to reduce mirror fouling due to soot from the experiment.

The modulated injection current was controlled using a commercial laser driver controller and interfaced using a computer-controlled function generator created in LabVIEW (using an NI PXIe 6386 DAQ module). The fitting routine uses line-by-line spectral simulations (using parameters from the HITRAN database [26]) which are remapped using the non-linear characterization of the laser, incorporating a background sample to create a 'simulated' measurement. Both the experimentally-obtained and simulated measurement are processed to find the second harmonic ($2f$) normalized by the first harmonic ($1f$), often called $2f/1f$-WMS [50]. This process is adjusted for varying concentration in the simulated measurement until convergence with the experimental measurement; an example fit is shown in Figure 8.

Some deviations are observed in Fig. 8 between the measurements and the fits; for CH_4 and C_2H_2, the line center and height of the measured feature vary from the fit and simulation near 1.3 ms and 0.3 ms, respectively. These deviations arise from some scan-to-scan variation in laser output caused by mode-hops in the 2.98 µm ICL, but are otherwise manageable in the fit. For the measurements of HCN, the fitted feature was measured near the lasing threshold of the ICL, resulting in a deviation in laser response that was not captured in the initial laser characterization; this is the reason for the measurement deviation observed only in the left feature in the $2f/1f$ signal for HCN. Despite this deviation; the targeted feature of HCN is spectrally isolated from C_2H_2. Representative time-resolved species measurements are shown in Figure 9 for C_2H_2, CH_4, and HCN.

The sensor sampled directly from the top slit of the compartment, using stainless steel tubing and a single coarse filter to sample the gas, while the sensor sat on the floor around 6' away. Similar to the production of benzene and ethylene (see Fig. 6), the duration of the methane and acetylene emissions were likely a function of the charring tendency of the fuels in each crib. Nylon, followed by MDF produced more emissions because these fuels contained components (nylon sticks, or MDF binder materials) that did not char and provided more burnt fuel mass. CH_4 was present in the highest concentration in the MDF and wood/nylon experiments, although was the least sensitive species for this optical sensor with a detection limit near 0.3%. For both HCN and C_2H_2, the sensor was more sensitive with a theoretical detection limit near 10 and 30 ppm respectively. Although these species have low detection limits, error caused by spectral convolution and etalon varied the results of the measurements at these lower concentrations; for this reason no measureable HCN was detected from MDF or wood.

A Monte Carlo analysis was conducted to estimate the uncertainty and sensitivity of the emission results due to the variations in specific experimental inputs such as pressure, temperature, pathlength, interfering species and

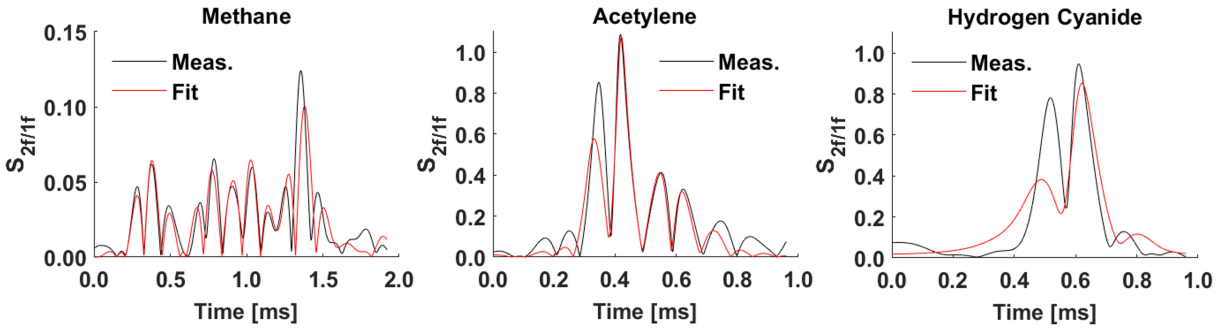

Figure 8: Comparison of the $2f/1f$ measurement to the fitting routine output.

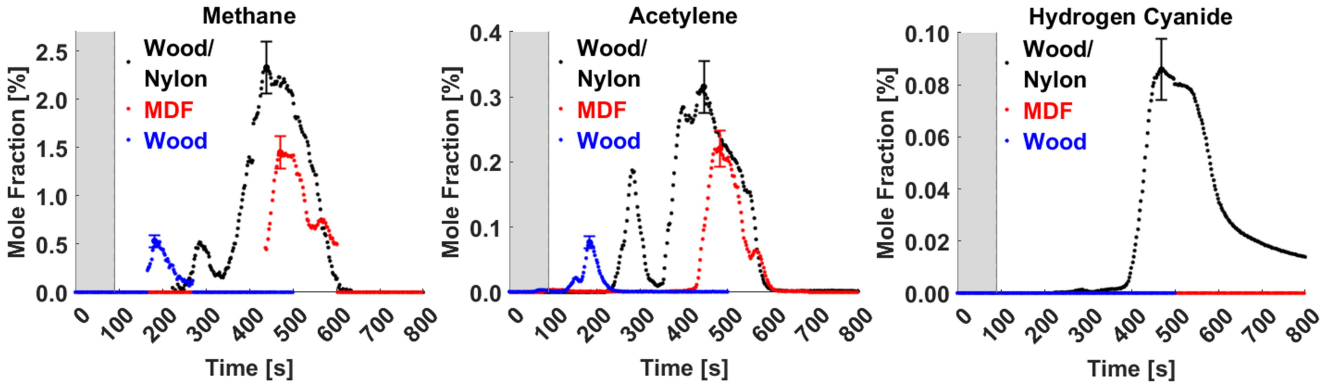

Figure 9: Concentration profiles of CH_4, C_2H_2, and HCN in time for the three fuels. The uncertainty in the concentration measurements are shown by the error bars. The grey shaded region indicates when the propane burner was on.

linestrength; the relative uncertainty was found to range between 12% and 15% for HCN, C_2H_2, and CH_4.

4. Discussion and Analysis

4.1. Species Yield Measurements

The yield (mass basis) of each species (i), Y_i was calculated with Eq. 5 using the collected species molar fraction and exiting flow measurements. Specifically, Y_i was calculated as the total mass of each species exiting the compartment divided by the average mass lost for the particular crib of interest.

$$Y_i = \left(\frac{\mathrm{Mw}_i}{\mathrm{Mw}_{air} m_{\mathrm{crib}} (1 - Y_{res})} \right) \int \dot{m}_{\mathrm{out}}(t)\ X_i(t) dt \quad (5)$$

Here m_{crib} is the average initial mass of the crib and Y_{res} is the fraction of mass remaining in the solid phase after flaming combustion ends. Y_{res} was calculated for each fuel using the initial and remaining crib masses for an experiment. The Y_{res} used in this analysis are the averaged fraction of three repeat experiments: 0.050±0.002, 0.164±0.009, and 0.13±0.01 for wood/nylon, MDF, and wood respectively. The mass of each exiting species was calculated by integrating the time-dependent measurements of the mass flow out of the compartment, $\dot{m}_{\mathrm{out}}$, and species mole fraction X_i using the trapezoidal rule. Then multiplying this resulting integration by the ratio of the molecular weights (Mw) of species i and air. The mass flow out, $\dot{m}_{\mathrm{out}}$, was calculated using Eq. 4. Figure 10 shows the raw temperature and pressure differential measurements and the resulting mass flow out measurement for a representative experiment.

The yield for each species was calculated using the flow and species measurement during the same experiment when possible. The corresponding flow and species measurements were used for every yield calculation, except for C_6H_6 and C_2H_2 from the wood crib, as flow measurements were not available. Instead the average of the mass flow measurements from 10 other replicate wood crib experiments were used. Although the burning behavior of wood is complex and very variable, as was seen in the large variation in repeated species concentration measurements, the mass flow measurements for this set of experiments are repeatable (Fig. 11). All of the mass flow out measurements for the wood experiments are within the uncertainty of the measurement. This shows that using the average mass flow measurement should capture the actual mass flow. Thus, using the average mass flow out to calculate the yield for experiments where mass flow data could not be collected, although not ideal, is reasonable. The uncertainty in the species yield measurements accounts for the uncertainty in X_i, T, ΔP, k, slit dimensions, m_{crib}, and Y_{res} measurements (see Appendix A).

Table 2 and Figure 12 present the yields for the three fuels. Generally, the yield for each species was highest for the wood/nylon crib. During the wood/nylon experiments, a small amount of smoke was observed to intermittently exit from the lower slit during a portion of the test. This

Table 2
Yields (g/g) of species from burning each fuel. Yields are reported as averages and plus/minus measurement uncertainty.

Fuel	CO $\times 10^{-3}$	CO_2 $\times 10^{-1}$	HCN $\times 10^{-3}$	C_6H_6 $\times 10^{-3}$	C_2H_4 $\times 10^{-3}$	C_2H_2 $\times 10^{-3}$	CH_4 $\times 10^{-3}$	Meas. HC† $\times 10^{-2}$
Wood/Nylon	7.8 ± 2.7	8.5 ± 3.0	7.2 ± 1.8	16 ± 3	43 ± 7	14 ± 3	59 ± 11	13 ± 2
MDF	3.7 ± 0.8	6.0 ± 1.5	0‡	4.4 ± 0.7	3.1 ± 0.5	3.5 ± 0.5	16 ± 2	2.7 ± 0.4
Wood	2.9 ± 1.2	5.2 ± 2.1	0‡	3.5 ± 1.1	0.5 ± 0.1	1.5 ± 0.3	2.5 ± 1.3	0.8 ± 0.2

† Meas. HC, short for measured hydrocarbons, is the combined yield of C_6H_6, C_2H_4, C_2H_2, and CH_4
‡ HCN was not detected in the wood and MDF experiments

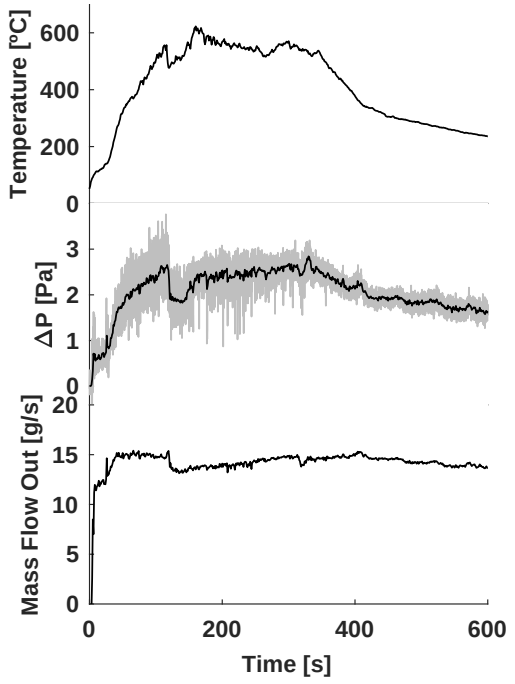

Figure 10: Representative mass flow out experimental measurements and resulting mass flow out (bottom) for a wood crib experiment. The top plot shows the raw temperature measurements. And the middle plot includes the raw (grey) and smoothed (black) differential pressure measurements.

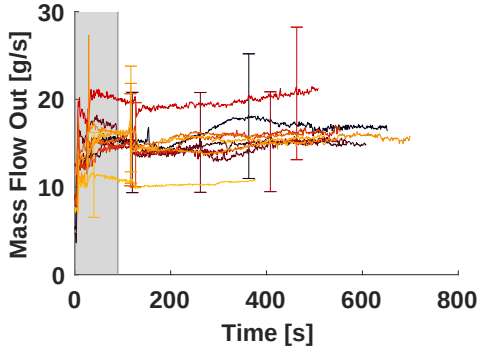

Figure 11: All wood mass flow out measurements with error bars showing measurement uncertainty. The grey shaded region indicates when the propane burner was on.

is attributed to the impact of the nylon melting on the fire behavior. As the crib burned, the nylon melted and formed small pool fires at the bottom of the compartment, increasing the exposed fuel surface area and consequently the burning rate, resulting in a lower smoke layer interface. This behavior was observed by the increased fluctuations in the inlet flow measurement collected during the wood/nylon experiments and visual observations of the vent during the test. The uniform one-way flow assumption for the lower slit is not fully characteristic of the wood/nylon experiments, because of the intermittent periods of two-way flow. Some of the combustion gases exited through the lower slit during this period, but the vast majority of the combustion gases exited through the upper slit. Furthermore, the periods of two-way flow in the lower slit were brief. Thus, continuing to use the assumption of uniform one-way flow in both slits for the yield calculation should only result in a slight underprediction of the species yields for the wood/nylon experiments.

The measured yields of CO and CO_2 each stayed within the same respective order of magnitude for the three fuels. The yield of CO was on the order of magnitude of $\mathcal{O}(10^{-3} - 10^{-2})$, while the yield of CO_2 was $\mathcal{O}(10^{-1} - 10^{0})$. As expected, these yields for CO are smaller than yields obtained from a small-scale test, the ISO TS19700 steady-state tube furnace, because of differences in how the fuel mass is considered (denominator of Eq. 5). In the present study, the total mass burned throughout the entire experiment was used, while other methods considered a dynamic mass loss rate. When using a dynamic mass loss rate the yields can be calculated for a particular duration of the experiment, but due to constraints in the experiment in this study, only overall yields were measured. Furthermore, unlike the tube furnace method, this experiment features a crib fire that will initially burn under well-ventilated conditions before progressing to under-ventilated conditions as smoke accumulates in the compartment, displacing oxygen. In contrast, the tube furnace method typically prescribes a specific ventilation condition by changing the flow rate of air through the furnace, resulting in steady conditions.

During each experiment, the temperature inside the compartment exceeded 600°C and flames extended out of the upper vent. This aligned with a rise in concentration of CO and the measured hydrocarbons, marking the transition from well-ventilated to under-ventilated conditions. The measured yield of CO is two orders of magnitude smaller than under-ventilated ISO TS19700 steady state tube furnace and large scale measurements [7, 31]. This is because the yield of CO is dependent on the availability of oxygen. At

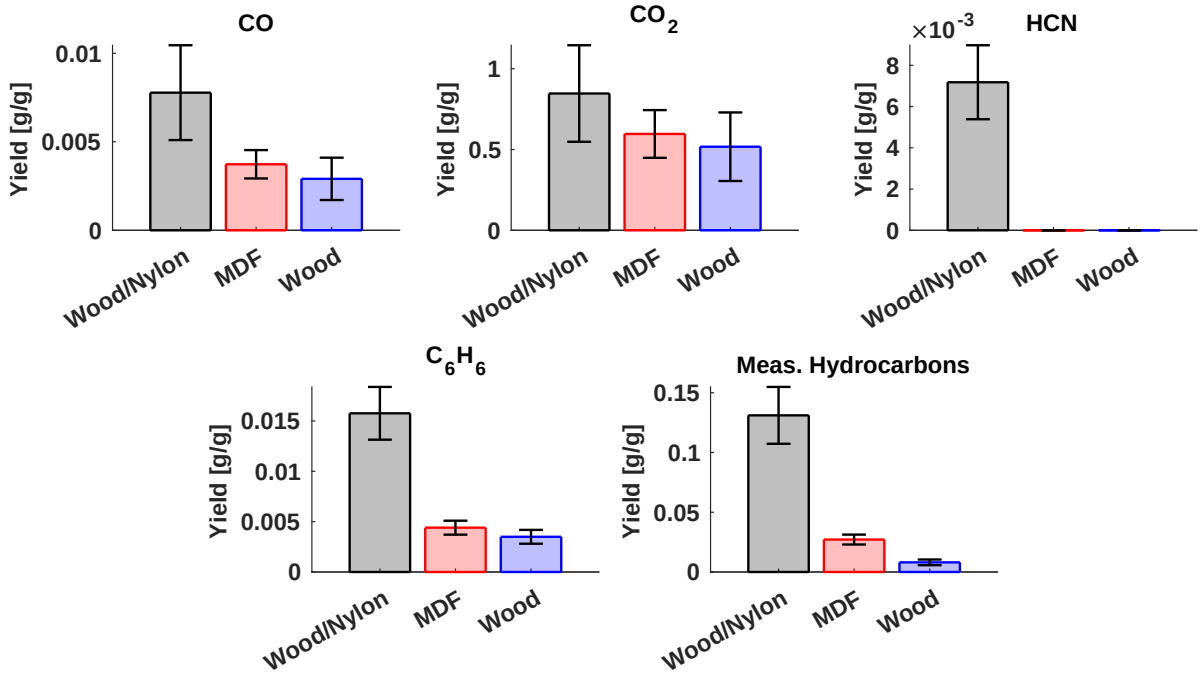

Figure 12: Yields with the measurement uncertainty of CO, CO_2, HCN, C_6H_6, and measured hydrocarbons from each fuel. The yield of measured hydrocarbons is the combined yield of C_6H_6, C_2H_4, C_2H_2, and CH_4

the start of the experiment little CO was produced. This period of well-ventilated combustion was included in the yield calculation, resulting is a lower yield of CO than if only the period of under-ventilated combustion was included in the analysis. Steady-state tube furnace measurements have found the yield of CO_2 to be slightly less than the stoichiometric yield of CO_2 under well-ventilated conditions and then decrease as ventilation is limited, typically remaining just above ~1 g/g [7]. The measured CO_2 yields of the present study are smaller, but similar in magnitude. The combined yield of measured hydrocarbons was highest for the wood/nylon tests, while the MDF and wood tests had similar yields one order of magnitude smaller than the wood/nylon yields. The measured yield of C_6H_6 (included in the combined measured hydrocarbon yield) for wood was 0.0035 g/g, which is similar to the instantaneous peak yield of around 0.009 g/g during an under-ventilated phase of a compartment fire with wood cribs [12].

HCN was only observed during the wood/nylon tests, and the average yield was 0.0072 g/g. This is probably because the concentration of HCN was below the detection limit for the wood and MDF experiments. Unlike the other fuels, nylon has nitrogen in its chemical structure, making it possible to emit more HCN if it is not fully oxidized. Wood and MDF each contain a much smaller amount of nitrogen (0.14% and 3.69% respectively) than nylon (11.86%) [5]. One study found the yield of HCN from nylon is an order of magnitude higher than that of MDF for under-ventilated tube furnace and large-scale compartment fire experiments [8]. The measured yield of HCN for the wood/nylon tests from the present study is between those from pure MDF and nylon experiments in Ref. [8].

4.2. Contribution of Toxicants to Tenability

A simple tenability calculation was performed to understand the relative contribution of measured toxicants towards the toxicity of the air in a nearby room contaminated by the emitted gases or a room in post-fire conditions that may still have combustion products lingering. For this analysis, the Fractional Irritant Concentration, FIC, and the fractional effective dose for incapacitation, F_{IN} including the Fractional Lethal Dose for irritants (FLD) and asphyxiation was calculated for a gas mixture assumed to be equal parts (by mass) fire effluents and air. In this scenario the combustion products would mix with and contaminate the air, and thus diluting the combustion product stream (i.e., measurements from the experiments). The exact level of dilution would depend on the specifics of the scenario (room size, mass flow rate in of the under-ventilated combustion products, ventilation of the room, etc.)[51, 52]. For a given configuration, the exact dilution level can be estimated using fire modeling tools such as Fire Dynamics Simulator (FDS) [53] and Consolidated Fire and Smoke Transport (CFAST) [54]. Here the case where the fire products are diluted with equal parts air (by mass) is considered. The exact dilution level is somewhat arbitrarily chosen, but is intended to be a plausible example scenario. In contrast, it is possible to calculate the tenability of the exhaust gas stream as measured directly, however the thermal hazard alone (gas temperatures up to ≈600°C, see Fig. 10) presented by this gas stream is sufficient to cause death quickly. Moreover, the terms in FED calculation are

non-linear with respect to species concentration. Thus, performing tenability calculations for the non-diluted product stream are likely not representative of scenarios of interest where the tenability would be ambiguous without detailed knowledge of the gas species composition.

With the fractional effective dose method, the tenability of a space can be determined based on the effects of heat, smoke, and toxic gas effects, irritants or asphyxiants [55, 56]. A space will be untenable if the fractional effective dose for any one of these parameters meets or exceeds 1. Exposure to this threshold will result in incapacitation or death for the average person. Therefore, for design and regulatory purposes a lower threshold should be used depending on the population of interest (a threshold of 0.3 is often used [55]). This analysis is limited to the effects of toxic gases and does not consider factors such as heat exposure. The fractional effective dose (FED) can be written generally for multiple species considering actual concentration, $C_i(t)$, the threshold concentration, C_{thresh}, and exposure time, t_{exp} to species i according to the equation

$$\mathrm{FED} = \int_{t_1}^{t_2} \sum_{i=1}^{n} \frac{C_i(t)}{(C_{thresh} t_{exp})_i} \Delta t \tag{6}$$

This concept has been applied to specific toxicants and exposure limits such as incapacitation. One of these is the combined fraction irritant concentration (FIC), which accounts for the additive effects of all irritants present, assuming that the effects are directly additive for each species i (Eq. 7).

$$\mathrm{FIC} = \sum \mathrm{FIC}_i \tag{7}$$

For this analysis C_6H_6 is the only measured species that is an irritant, therefore $\mathrm{FIC} = \mathrm{FIC}_{C_6H_6}$. Using the general FED equation (Eq. 6), $\mathrm{FIC}_{C_6H_6}$ can be evaluated.

$$\mathrm{FIC}_{C_6H_6} = \int_{t_1}^{t_2} \frac{X_{C_6H_6}(t)}{(X_{thresh} t_{exp})_{C_6H_6}} \Delta t \tag{8}$$

where $X_{C_6H_6}$ is the average molar fraction of C_6H_6 at time t over time Δt, and $(X_{thresh} t_{exp})_{C_6H_6}$ is the exposure dose, which is the product of the relevant threshold mole fraction and the exposure time. In this case, the Acute Exposure Guideline Level (AEGL) 2 (1100 ppm × 30 min) was used [57], which corresponds to the threshold exposure level where permanent injury or incapacitation occurs for the average person.

The tendency for incapacitation can similarly be calculated using the fractional effective dose for incapacitation, F_{IN}, which accounts for exposure time and additive effects of the presence of multiple asphyxiants and irritant gas species, that results in incapacitation due to asphyxiation [55, 56]. F_{IN} is calculated as

$$F_{\mathrm{IN}} = (F_{\mathrm{I_{CO}}} + F_{\mathrm{I_{CN}}} + F_{\mathrm{I_{NOx}}} + \mathrm{FLD_{irr}}) \times V_{\mathrm{CO_2}} + F_{\mathrm{I_O}} \tag{9}$$

where F_{I_i} are the fractional effect dose for incapacitation by the species, i. CN is the effect associated with HCN. $V_{\mathrm{CO_2}}$ accounts for the effect of elevated CO_2 concentrations on respiration, which is calculated as

$$V_{\mathrm{CO_2}} = \exp\left(\frac{[\%\mathrm{CO_2}]}{5}\right) \tag{10}$$

where the concentration of CO_2 is in volume percent. $\mathrm{FLD_{irr}}$ is the fractional lethal does of irritants. $\mathrm{FLD_{irr}}$ was calculated the same as FIC, except the corresponding threshold for death (AEGL 3) for benzene was used (5600×30 ppm min). The effects of nitrogen oxides, $F_{\mathrm{I_{NO_x}}}$, and lack of oxygen, $F_{\mathrm{I_{O_2}}}$, were excluded because concentration measurements were not collected for these species. The effects of CO and HCN concentration were accounted for using Equations 11 and 12.

$$F_{\mathrm{I_{CO}}} = 3.317 \times 10^{-5} \cdot [\mathrm{CO}]^{1.036} \frac{\dot{V}(t)}{D} \tag{11}$$

$$F_{\mathrm{I_{CN}}} = \frac{[\mathrm{CN}]^{2.36}}{1.2 \times 10^{6}}\, t \tag{12}$$

where the volumetric concentrations of CO and HCN are in ppm, $\dot{V}$ is the volume flow rate of air breathed by the individual in lpm, D is the exposure dose for incapacitation for CO in the blood in %COHb and t is the duration of the exposure in minutes. For this case the values corresponding to *"hard work"* of 50 lpm and 20%COHb were used [55]. An exposure duration of 30 minutes was selected, because it is a commonly used exposure period for toxicity analysis. Many toxicity metrics for different gas species including AEGL and the lethal concentration for 50% of the population (LC_{50}) are available for 30 minute exposure periods and FED based on 30 minute exposure periods have previously been used to compare the toxicity of different fuels and burning conditions [1].

The molar concentrations of each species in a 1:1 by mass diluted mixture of fire effluents to air was used for this analysis. Equation 13 was used to calculate the molar concentration using the total yields, assuming that the molecular weight of the mixture is the same as air and that the flow of fire effluents before dilution is the average mass flow out of the compartment for each fuel.

$$x_{i,\mathrm{mix}} = \frac{1}{R_D + 1}\left(\frac{\mathrm{Mw_{air}}}{\mathrm{Mw}_i} \frac{Y_i m_{\mathrm{crib}}(1 - Y_{res})}{t_{burn}\, \dot{m}_{\mathrm{out,avg}}} + R_D x_{i,\mathrm{air}}\right) \tag{13}$$

The dilution ratio, $R_D = 1$, is the ratio by mass of fresh air to fire effluents from the reduced scale compartment. The mass burned of the crib, average mass flow out of the compartment ($\dot{m}_{\mathrm{out,avg}}$), and the average duration of the experiments (t_{burn}) were used to calculate the mass fraction of each species in the fire effluent from the total yield. t_{burn} was 18.2 min for wood/nylon, 14.2 min for MDF, and 9.2 min for wood. The molar concentration of each species in the diluted mixture $x_{i,\mathrm{mix}}$ was then calculated given the assumed dilution ratio and the ambient concentration of each species in the air ($x_{i,\mathrm{air}}$). $x_{i,\mathrm{air}}$ for CO_2, CO, HCN, and C_6H_6 were assumed to be 0.04%, 0, 0, and 0 respectively.

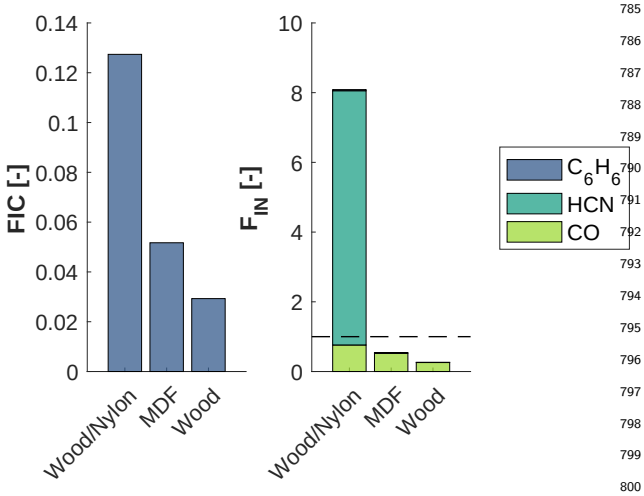

Figure 13: Estimated fractional effective dose for incapacitation due to sensory irritants (left) and asphyxiation (right), if compartment combustion products are diluted at a 1:1 mass ratio of fresh air to fire effluents. This analysis considers the influence of CO, CO_2, HCN, and C_6H_6 concentration effects. The contribution of CO_2 is accounted for in F_{IN} as an effect on the ventilation rate. C_6H_6's contribution to F_{IN} for all fuels is small and cannot be visually seen.

Figure 13 compares the contribution of CO, HCN, and C_6H_6 considering CO_2 hyperventilation. For this dilution ratio, the predicted gas mixtures from burning wood and MDF would have FED values less than 1, but MDF would have a FED value greater than 0.3 (an upper limit often used for fire protection analysis [55]). Notably, the inclusion of non-wood components results in a much higher toxicity compared to the case with the wood and MDF cribs. The F_{IN} for the wood/nylon crib greatly exceed 1, indicating the gas mixture is very toxic. These calculations provide insight into how the fuels involved impact the toxicity of the fire effluents. These results should not be applied to real scenarios without considering situation specific aspects such as fire induced flows in rooms, the fire development, among other factors.

HCN was the largest contributor to the F_{IN} for the wood/nylon cribs. HCN makes up the majority of the F_{IN} for this fuel, which is similar to the contribution of the HCN to the FED for nylon burning in under-ventilated conditions reported by Stec in [1]. CO had the largest contribution to the F_{IN} for wood and MDF and the second largest for wood/nylon cribs. The contribution of C_6H_6 towards the F_{IN} is small for all the fuel types, but was the largest for wood/nylon.

5. Conclusions

Emissions of several toxicant and incomplete-combustion species (CO, CO_2, HCN, C_6H_6, CH_4, C_2H_2, and C_2H_4) from under-ventilated burning cribs of different fuels (wood, MDF, and nylon) was investigated using FTIR and advanced tunable laser absorption spectroscopy methods. LAS was able to perform 1 Hz measurements with no smoke sample pre-conditioning while FTIR measurements were performed at 0.03 Hz with significant pre-conditioning of the sampled gases. This time resolution allowed for measurement of emissions of reduced-scale compartment fire experiments during different phases of the fire development. This measurement capability and experimental configuration presents an opportunity for high-throughput testing of various fuel loads including composites under different fire conditions. Using flow and species concentration measurements, yields of toxicant species were determined. The measured values exhibit similar trends, but some species differ from reported values from small- and large-scale fire experiments. Notably, the nylon/wood fuel packages resulted in much larger toxicant concentrations and yields, corresponding to over an 100% increase in toxicity. The LAS sensing methods combined with future improvements in measurement synchronization (e.g. simultaneous measurement of more species) may enable fully time-resolved toxicity metrics during fire evolution, and provide for more granular examination of the transient fire state during realistic fire progression. The current work and species measurements collected during these experiments provide valuable data on the chemical composition of gaseous combustion products released throughout a compartment fire and provide insight into the relative production rates of several hydrocarbon species.

6. Acknowledgments

This research was funded by the Federal Emergency Management Agency (FEMA) EMW-2021-FP-00199. KLF is partially supported by NSF Award 2339502 and NASA MIRO Cooperative Agreement 80NSSC19M0194. The authors acknowledge the assistance of Makayla A. Watts, Kevin Eisenbarger, Joshua Miller, Fredrick Brokaw leading up to- and during- the experiments. The authors acknowledge the assistance of Samy Rosenberg and Mahesh Kottalgi for assistance performing the experiments.

A. Uncertainty Analysis

An uncertainty analysis was completed to quantify the measurement uncertainty for each species concentration and yield measurements. The measurement uncertainty for each species concentration measurement was assessed and quantified individually, then combined with the other measurement uncertainties, and propagated through the yield calculation. The uncertainty was quantified for the yields of all species and the concentration measurements of CO, CO_2, C_6H_6, and C_2H_4, assuming that the function to calculate the yield or the concentration (q) is a function of several variables each with independent random errors. Therefore, the uncertainty can be quantified using the following general form [58].

$$\delta q = \sqrt{\left(\frac{\partial q}{\partial x}\,\delta x\right)^2 + \cdots + \left(\frac{\partial q}{\partial z}\,\delta z\right)^2} \tag{14}$$

The uncertainty of C_2H_2, CH_4, and HCN concentration measurements were quantified using Monte Carlo analysis. The following sections are a detailed description of the assumptions and analysis methods for assessed measurement.

A.1. CO and CO_2 Concentrations

The uncertainty of CO and CO_2 measurements were determined by evaluating the uncertainty in the variables of the Beer-Lambert Law (Equations 1 and 2). In the Beer-Lambert Law all the variables are multiplied together, therefore Eq. 14 can be simplified to Eq. 15 for cross sectional or Eq. 16 for line strength based measurements.

$$\left[\frac{\Delta X}{X}\right]_i = \sqrt{\left(\frac{\Delta P}{P}\right)^2 + \left(\frac{\Delta T}{T}\right)^2 + \left(\frac{\Delta \sigma}{\sigma}\right)^2 + \left(\frac{\Delta \alpha}{\alpha}\right)^2 + \left(\frac{\Delta L}{L}\right)^2} \tag{15}$$

$$\left[\frac{\Delta X}{X}\right]_i = \sqrt{\left(\frac{\Delta P}{P}\right)^2 + \left(\frac{\Delta S}{S}\right)^2 + \left(\frac{\Delta \alpha}{\alpha}\right)^2 + \left(\frac{\Delta L}{L}\right)^2} \tag{16}$$

where the uncertainty in pressure is $\Delta P/P$, temperature $\Delta T/T$, cross sections $\Delta\sigma/\sigma$, absorbance $\Delta\alpha/\alpha$, pathlength $\Delta L/L$, and line strength $\Delta S/S$.

Equation 16 was used to calculate the uncertainty in the concentration of CO and CO_2, since the concentrations were evaluated using line strength. For the analysis, it was assumed that $\Delta P/P$ was 20%, and that $\Delta L/L$ is 0.75%. $\Delta S/S$ was the reported relative line strength uncertainty for the HITRAN spectral data. The rounded-up average relative line strength uncertainty was used, which was 2% for CO and 10% for CO_2. In each spectral analysis region the root mean squared absorbance was $\Delta\alpha$ and the maximum absorbance was α. The reported measurement uncertainty in the concentration of CO and CO_2 is the average relative uncertainty from three of the experiments, one of each fuel type. The relative uncertainty of all measurements for these three experiments was calculated and then averaged. The relative uncertainty was $[{}^{\Delta X}/_{X}]_{CO} = 0.24$ and $[{}^{\Delta X}/_{X}]_{CO_2} = 0.23$.

A.2. C_6H_6 and C_2H_4 Concentrations

Similarly, the uncertainty of the C_6H_6 and C_2H_4 concentration measurements were assessed using Eqs. 15 and 16 respectively. The uncertainty in pressure ($\Delta P/P = 0.0025$), temperature ($\Delta T/T = 0.0075$), and pathlength ($\Delta L/L = 0.0014$) were all specified by the respective manufacturers of the pressure transducers, thermocouples, and Herriott cell. The uncertainty in absorbance ($\Delta\alpha/\alpha$) for each temporal scan is quantified by dividing the minimum detectable absorbance ($\Delta\alpha$) by the peak absorbance (α) of either the C_6H_6 or the C_2H_4 fitting routine. The minimum detectable absorbance was quantified in a non-absorbing scan to be $\Delta\alpha = 0.003$. An uncertainty of 4.90% was calculated for the C_6H_6 cross sections ($\Delta\sigma/\sigma$). This was derived from the average variation between interpolated and measured optical cross sections across the sensor's pressure range. Not having access to uncertainty data for the linestrength of the chosen C_2H_4 lines, a conservative value of 20% was used for $\Delta S/S$. Note that there is no value for uncertainty of the lineshape (ϕ) because lineshape is an integrated parameter that always integrates to a value of unity.

A.3. C_2H_2, CH_4, and HCN Concentration

To quantify the uncertainty in the WMS measurements a Monte Carlo analysis was conducted varying specific experimental inputs such as pressure, temperature, pathlength, linestrength, and interfering species concentration. The total number of iterations conducted for the Monte Carlo for HCN, C_2H_2, and CH_4 were 2000, split evenly at 8 varying time/concentrations throughout a single test to account for any variations in interferer species concentration during the test. The largest contributor to the uncertainty was the pathlength, which was given a conservative experimentally found uncertainty of ±5 cm.

The relative uncertainties for HCN, CH_4, and C_2H_2 was between 12%–14% with its highest uncertainty being above 15% for HCN near the detection limit, and the lowest uncertainty seen was 10.5% for CH_4 near 400 s. For the CH_4 concentration measurement, the CH_4 spectra is partially overlapping with an interfering transition of C_2H_2 (not the targeted feature used to measure C_2H_2 in this study), which adds to the uncertainty of the CH_4 measurement. This additional uncertainty needs to be considered, since this CH_4 concentration uncertainty is a function of both CH_4 and C_2H_2 mole fraction. To estimate this influence, the uncertainty was conservatively increased from 15% to 20% based on comparison of independently-conducted optical gas cell measurements obtained by the WMS model against known barometrically-prepared mixtures of CH_4 and C_2H_2. This uncertainty calculated in the Monte Carlo analysis for CH_4 was found to be near 12% throughout the measurement at all concentrations. The resulting increase in CH_4 concentration uncertainty was marginal, with a relative 20% uncertainty at lower concentrations, which reduced to a relative uncertainty of 15% at higher concentrations.

A.4. Yields

The measured yield for each species is a function of many variables. For this analysis, the uncertainty in fuel mass, residue fraction, slit width (w), slit height (h), s-type pitot tube probe coefficients, temperature measurements, differential pressure measurements, and concentration measurements were considered. Therefore, the uncertainty can

be quantified using Eq. 17, if it is assumed that the uncertainty of each of these variables is independent and random.

$$(\delta Y_i)^2 = \left(\frac{\partial Y_i}{\partial m_{\text{crib}}}\delta m_{\text{crib}}\right)^2 + \left(\frac{\partial Y_i}{\partial Y_{res}}\delta Y_{res}\right)^2 + \left(\frac{\partial Y_i}{\partial w}\delta w\right)^2 + \left(\frac{\partial Y_i}{\partial h}\delta h\right)^2 + \sum_{j=1}^{n}\left(\frac{\partial Y_i}{\partial k_j}\delta k_j\right)^2 + \sum_{j=1}^{n}\left(\frac{\partial Y_i}{\partial T_j}\delta T_j\right)^2 + \sum_{j=1}^{n}\left(\frac{\partial Y_i}{\partial(\Delta P_j)}\delta(\Delta P_j)\right)^2 + \sum_{j=1}^{n}\left(\frac{\partial Y_i}{\partial X_{i,j}}\delta X_{i,j}\right)^2 \quad (17)$$

where j is the index that specifies the measurement for a specific time, where $j = 1$ is at ignition and $j = n$ is the end of the experiment. The partial derivatives of the yield with respect to each variable were determined using automatic differentiation, because of the number of variables and the complexity of the function used to calculate the yield.

The uncertainty of the average crib mass (δm_{crib}) and the residue fraction (δY_{res}) was the standard deviation of repeated measurements. The uncertainty in the slit width (δw) and height (δh) was 0.5 cm, which accounts for the non-uniformity of the slit. The uncertainty in the s-type pitot tube probe coefficient (δk) was determined through calibration measurements to be 0.338 Pa. The uncertainty reported by the manufacture of the measurement devices for temperature (δT) and differential pressure ($\delta(\Delta P)$) were used.

References

[1] Anna A. Stec. Fire toxicity – the elephant in the room? *Fire Saf. J.*, 91:79–90, 2017. doi: 10.1016/j.firesaf.2017.05.003.

[2] Alexander C. Mayer, Kenneth W. Fent, Andrea F. Wilkinson, I-Chen Chen, Miriam R. Siegel, Christine Toennis, Deborah Sammons, Juliana Meadows, Richard M. Kesler, Steve Kerber, Denise L. Smith, Farzaneh Masoud, Deepak Bhandari, Yuesong Wang, Benjamin C. Blount, Antonia M. Calafat, and Gavin P. Horn. Evaluating Exposure to VOCs and Naphthalene for Firefighters Wearing Different PPE Configurations through Measures in Air, Exhaled Breath, and Urine. *Int. J. Environ. Res. Public Health*, 20(12), 2023. doi: 10.3390/ijerph20126057.

[3] Alexander C. Mayer, Kenneth W. Fent, Andrea Wilkinson, I-Chen Chen, Steve Kerber, Denise L. Smith, Richard M. Kesler, and Gavin P. Horn. Characterizing Exposure to Benzene, Toluene, and Naphthalene in Firefighters Wearing Different Types of New or Laundered PPE. *International Journal of Hygiene and Environmental Health*, 240:113900, 2022. doi: 10.1016/j.ijheh.2021.113900.

[4] Daniel T. Gottuk and Brain Y. Lattimer. Effect of combustion conditions on species production. In Morgan J. Hurley, editor, *SFPE Handbook of Fire Protection Engineering*, volume 2, pages 486–528. Springer, New York, 5 edition, 2016. doi: 10.1007/978-1-4939-2565-0.

[5] David A. Purser. Toxic combustion product yields as a function of equivalence ratio and flame retardants in under-ventilated fires: Bench-large-scale comparisons. *Polymers*, 8(9), 2016. doi: 10.3390/polym8090330.

[6] Gordon E. Hartzell. Overview of combustion toxicology. *Toxico.*, 115 (1):7–23, 1996. doi: 10.1016/S0300-483X(96)03492-0. International Colloquium on Advances in Combustion Toxicology.

[7] David A. Purser. Combustion toxicity. In Morgan J. Hurley, editor, *SFPE Handbook of Fire Protection Engineering*, volume 2, pages 2207–2307. Springer, New York, 5 edition, 2016. doi: 10.1007/978-1-4939-2565-0.

[8] David Purser and Jenny Purser. Hcn yields and fate of fuel nitrogen for materials under different combustion conditions in the iso 19700 tube furnace and large -scale fires. *Fire Saf. Sci.*, 9:1117–1128, 01 2008. doi: 10.3801/IAFSS.FSS.9-1117.

[9] A. A. Stec, T. R. Hull, K. Lebek, J. A. Purser, and D. A. Purser. The Effect of Temperature and Ventilation Condition on the Toxic Product Yields from Burning Polymers. *Fire and Materials*, 32(1):49–60, 2008. doi: 10.1002/fam.955.

[10] Iben Hansen-Bruhn and T. Richard Hull. Smoke Toxicity of Fire Protecting Timber Treatments. *Fire Safety Journal*, 141:103977, 2023. doi: 10.1016/j.firesaf.2023.103977.

[11] Per Blomqvist and Anders Lönnermark. Characterization of the Combustion Products in Large-scale Fire Tests: Comparison of Three Experimental Configurations. *Fire and Materials*, 25(2):71–81, 2001. doi: 10.1002/fam.761.

[12] Omar Aljumaiah, Gordon Andrews, Bintu Mustafa, H. Al-qattan, V. Shah, and Roth Phylaktou. Air starved wood crib compartment fire heat release and toxic gas yields. *Fire Saf. Sci.*, 10:1263–1276, 01 2011. doi: 10.3801/IAFFS.FSS.10-1263.

[13] A Alarifi, HN Phylaktou, GE Andrews, J Dave, and O Aljumaiah. Toxic Gas Emissions from a Timber-Pallet-Stack Fire in a Full-Scale Compartment, 2017.

[14] Bronwyn Forrest, Alexander DiPaola, Vusal Ibrahimli, Ayaan Lakhani, and Elizabeth Weckman. Towards Characterizing Full-scale Furniture Fires in a Two-storey House: Gaseous Species Concentrations during a Ventilation-limited Fire. *Fire Safety Journal*, 141: 103963, 2023. doi: 10.1016/j.firesaf.2023.103963.

[15] Thermo Scientific. FT-IR Sampling Parameters for Exhaust Gas Measurements, 2007. Technical Note: 50650.

[16] Anna A. Stec, Peter Fardell, Per Blomqvist, Lucas Bustamante-Valencia, Laurent Saragoza, and Eric Guillaume. Quantification of Fire Gases by FTIR: Experimental Characterisation of Calibration Systems. *Fire Safety Journal*, 46(5):225–233, 2011. doi: 10.1016/j.firesaf.2011.02.004.

[17] Nima Afshar-Mohajer, Christopher Zuidema, Sinan Sousan, Laura Hallett, Marcus Tatum, Ana M. Rule, Geb Thomas, Thomas M. Peters, and Kirsten Koehler and. Evaluation of Low-cost Electrochemical Sensors for Environmental Monitoring of Ozone, Nitrogen Dioxide, and Carbon Monoxide. *Journal of Occupational and Environmental Hygiene*, 15(2):87–98, 2018. doi: 10.1080/15459624.2017.1388918.

[18] Ronald K. Hanson, R. Mitchell Spearrin, and Christopher S. Goldenstein. *Spectroscopy and Optical Diagnostics for Gases*. 2016. doi: 10.1007/978-3-319-23252-2.

[19] Jane Hodgkinson and Ralph P. Tatam. Optical Gas Sensing: A Review. *Measurement Science and Technology*, 24, 2013. doi: 10.1088/0957-0233/24/1/012004.

[20] Christopher S. Goldenstein, R. Mitchell Spearrin, Jay B. Jeffries, and Ronald K. Hanson. Infrared laser-absorption sensing for combustion gases. *Progress in Energy and Combustion Science*, 60:132–176, 2017. ISSN 03601285. doi: 10.1016/j.pecs.2016.12.002. URL http://dx.doi.org/10.1016/j.pecs.2016.12.002.

[21] Tingdong Cai, Guangzhen Gao, Minrui Wang, Guishi Wang, Ying Liu, and Xiaoming Gao. High-pressure measurements of temperature and CO_2 concentration using tunable diode lasers at 2μm. *Applied*

Spectroscopy, 70:474–484, 3 2016. ISSN 19433530. doi: 10.1177/0003702815626672.

[22] Qing Li, Feiyu Ji, Wei Wang, Liuhao Ma, and Yu Wang. A mid-infrared laser absorption sensor for calibration-free measurement of nitric oxide in laminar premixed methane/ammonia cofired flames. *Microwave and Optical Technology Letters*, 66, 1 2024. ISSN 10982760. doi: 10.1002/mop.33815.

[23] Kevin K. Schwarm, Anil P. Nair, Chuyu Wei, R. Mitchell Spearrin, Emre Ozen, Edward Gonzalez, and Jason Kriesel. Three-dimensional real-time mapping of CO and CO_2 concentrations in active forest burns with a uav spectrometer. *AIAA Science and Technology Forum and Exposition, AIAA SciTech Forum 2022*, pages 1–9, 2022. doi: 10.2514/6.2022-2291.

[24] Yunyong Utiskul, James G. Quintiere, Ali S. Rangwala, Brian A. Ringwelski, Kaoru Wakatsuki, and Tomohiro Naruse. Compartment Fire Phenomena under Limited Ventilation. *Fire Saf. J.*, 40(4):367–390, 2005. ISSN 0379-7112. doi: 10.1016/j.firesaf.2005.02.002.

[25] Giovanni Di Cristina and Rodney A. Bryant. Comparison of two flow measurement devices for use in fire experiments. *Proceedings of the Combustion Institute*, 40(1):105557, 2024. doi: 10.1016/j.proci.2024.105557.

[26] I. E. Gordon, L. S. Rothman, R. J. Hargreaves, R. Hashemi, E. V. Karlovets, F. M. Skinner, E. K. Conway, C. Hill, R. V. Kochanov, Y. Tan, P. Wcisło, A. A. Finenko, K. Nelson, P. F. Bernath, M. Birk, V. Boudon, A. Campargue, K. V. Chance, A. Coustenis, B. J. Drouin, J. M. Flaud, R. R. Gamache, J. T. Hodges, D. Jacquemart, E. J. Mlawer, A. V. Nikitin, V. I. Perevalov, M. Rotger, J. Tennyson, G. C. Toon, H. Tran, V. G. Tyuterev, E. M. Adkins, A. Baker, A. Barbe, E. Canè, A. G. Császár, A. Dudaryonok, O. Egorov, A. J. Fleisher, H. Fleurbaey, A. Foltynowicz, T. Furtenbacher, J. J. Harrison, J. M. Hartmann, V. M. Horneman, X. Huang, T. Karman, J. Karns, S. Kassi, I. Kleiner, V. Kofman, F. Kwabia-Tchana, N. N. Lavrentieva, T. J. Lee, D. A. Long, A. A. Lukashevskaya, O. M. Lyulin, V. Yu Makhnev, W. Matt, S. T. Massie, M. Melosso, S. N. Mikhailenko, D. Mondelain, H. S.P. Müller, O. V. Naumenko, A. Perrin, O. L. Polyansky, E. Raddaoui, P. L. Raston, Z. D. Reed, M. Rey, C. Richard, R. Tóbiás, I. Sadiek, D. W. Schwenke, E. Starikova, K. Sung, F. Tamassia, S. A. Tashkun, J. Vander Auwera, I. A. Vasilenko, A. A. Vigasin, G. L. Villanueva, B. Vispoel, G. Wagner, A. Yachmenev, and S. N. Yurchenko. The HITRAN2020 Molecular Spectroscopic Database. *Journal of Quantitative Spectroscopy and Radiative Transfer*, 277, 2022. doi: 10.1016/J.JQSRT.2021.107949.

[27] Yoshio Tsuchiya. Co/co_2 ratios in fire. *Fire Saf. Sci.*, 4:515–526, 1994. doi: 10.3801/IAFSS.FSS.4-515.

[28] D. Quang Dao, J. Luche, T. Rogaume, F. Richard, L. Bustamante Valencia, and S. Ruban. Polyamide 6 and polyurethane used as liner for hydrogen composite cylinder: An estimation of fire behaviours. *Fire Technology*, 52(2):397–420, Mar 2016. ISSN 1572-8099. doi: 10.1007/s10694-014-0423-4.

[29] Iben Hansen-Bruhn and T. Richard Hull. Flammability and burning behaviour of fire protected timber. *Fire Safety Journal*, 140:103918, 2023. ISSN 0379-7112. doi: 10.1016/j.firesaf.2023.103918.

[30] Yufeng Lai, Xuanqi Liu, Matthew Davies, Callum Fisk, Michael Holliday, David King, Yang Zhang, and Jon Willmott. Characterisation of wood combustion and emission under varying moisture contents using multiple imaging techniques. *Fuel*, 373:132397, 2024. ISSN 0016-2361. doi: 10.1016/j.fuel.2024.132397.

[31] Andrew Lock, Matthew Bundy, Erik L Johnsson, Anthony Hamins, Gwon Hyun Ko, Cheolhong Hwang, Paul Fuss, and Richard Harris. Experimental study of the effects of fuel type, fuel distribution, and vent size on full-scale underventilated compartment fires in an iso 9705 room. *NIST Technical Note*, 1603:53–54, 2008.

[32] D. H. Whiffen. Infra-red summation bands of the out-of-plane c-h bending vibrations of substituted benzene compounds. *Spectrochimca Acta*, 253:263, 1955. doi: 10.1016/0371-1951(55)80038-0.

[33] Mhanna Mhanna, Guangle Zhang, Noushad Kunnummal, and Aamir Farooq. Cavity-enhanced measurements of benzene for. 21:3849–3859, 2021. doi: 10.1109/JSEN.2020.3026981.

[34] R. Sur, Y. Ding, R. B. Jackson, and R. K. Hanson. Tunable laser-based detection of benzene using spectrally narrow absorption features. *Applied Physics B: Lasers and Optics*, 125, 11 2019. ISSN 09462171. doi: 10.1007/s00340-019-7311-z.

[35] Nicolas S. B. Jaeger, Yi Yan, and R. Mitchell Spearrin. Benzene and Carbon Monoxide Sensing in Urban Fire Environments via Tunable Interband Cascade Laser Absorption Spectroscopy. In Jacob Scheuer, editor, *Optical Sensing and Precision Metrology*, page 3. SPIE, 3 2025. doi: 10.1117/12.3042391.

[36] Steven W Sharpe, Timothy J Johnson, Robert L Sams, Pamela M Chu, George C Rhoderick, and Patricia A Johnson. Gas-phase databases for quantitative infrared spectroscopy, 2004. URL http://gases.nist.gov/spectral.html.

[37] T. Delahaye, R. Armante, N.A. Scott, N. Jacquinet-Husson, A. Chédin, L. Crépeau, C. Crevoisier, V. Douet, A. Perrin, A. Barbe, V. Boudon, A. Campargue, L.H. Coudert, V. Ebert, J.-M. Flaud, R.R. Gamache, D. Jacquemart, A. Jolly, F. Kwabia Tchana, A. Kyuberis, G. Li, O.M. Lyulin, L. Manceron, S. Mikhailenko, N. Moazzen-Ahmadi, H.S.P. Müller, O.V. Naumenko, A. Nikitin, V.I Perevalov, C. Richard, E. Starikova, S.A. Tashkun, Vl.G. Tyuterev, J. Vander Auwera, B. Vispoel, A. Yachmenev, and S. Yurchenko. The 2020 Edition of the GEISA Spectroscopic Database. *Journal of Molecular Spectroscopy*, 380:111510, 2021. doi: 10.1016/j.jms.2021.111510.

[38] Barathan Jeevaretanam, Mostafa Abuseada, Chuyu Wei, Nicolas Q. Minesi, Timothy S. Fisher, and R. Mitchell Spearrin. Transient analysis of solar pyrolysis and hydrogen yield via interband cascade laser absorption spectroscopy of methane, acetylene, ethylene, and ethane. *Applications in Energy and Combustion Science*, 16, 12 2023. ISSN 2666352X. doi: 10.1016/j.jaecs.2023.100223.

[39] Hilary R. Melroy, Erin M. Adkins, Maya J. Pause, and J. Houston Miller. Species measurements in a nitrogen-diluted, ethylene air diffusion flame using direct sampling mass spectrometry and tunable diode laser absorption spectroscopy. *Proceedings of the Combustion Institute*, 35:3749–3755, 2015. ISSN 15407489. doi: 10.1016/j.proci.2014.08.022.

[40] A. B. McLean, C. E.J. Mitchell, and D. M. Swanston. Implementation of an efficient analytical approximation to the voigt function for photoemission lineshape analysis. *J. Electron. Spectrosc. Relat. Phenom.*, 69:125–132, 1994. doi: 10.1016/0368-2048(94)02189-7.

[41] M. J. Berger, J. S. Coursey, M. A. Zucker, and J. Chang. ESTAR, PSTAR, and ASTAR: Stopping Power and Range Tables for Electrons, Protons, and Helium Ions. https://physics.nist.gov/Star, 2017. National Institute of Standards and Technology, Gaithersburg, MD.

[42] Forest Products Laboratory. *Wood Handbook: Wood as an Engineering Material*. General Technical Report FPL-GTR-190. U.S. Department of Agriculture, Forest Service, Forest Products Laboratory, Madison, WI, centennial edition edition, 2021.

[43] Natural Resources Canada. Medium-Density Fibreboard. https://natural-resources.canada.ca/forest-forestry/forest-industry-trade/medium-density-fibreboard, 2024. Accessed: 2025-04-22.

[44] Anna. Stec and T. Richard. Hull. *Fire toxicity / edited by Anna Stec and Richard Hull.* Woodhead Publishing in materials. CRC Press, Boca Raton, 2010. ISBN 9781845695026.

[45] Joshua W. Stiborek, Roy S. Ramirez, and Christopher S. Goldenstein. Development of a single-ended mid-infrared fiber-coupled laser absorption sensor for measurements of temperature, co, and co2 in harsh environments. *Appl. Opt.*, 63(29):7588, 10 2024. doi: 10.1364/AO.534027.

[46] Mohsin Raza, Liuhao Ma, Shunchun Yao, Longfei Chen, and Wei Ren. High-temperature dual-species (co/nh3) detection using calibration-free scanned-wavelength-modulation spectroscopy at 2.3 μm. *Fuel*, 305(July):121591, 2021. doi: 10.1016/j.fuel.2021.121591.

[47] Kyle L. Fetter, Laura Munera, Makayla A. Watts, and Daniel I. Pineda. Interband cascade laser absorption sensor for sensitive measurement of hydrogen chloride in smoke-laden gases using wavelength modulation spectroscopy. *Appl. Opt.*, 63(33):8517, nov 2024. doi:

10.1364/AO.540760.

[48] Wubin Weng, Marcus Aldén, and Zhongshan Li. Simultaneous quantitative detection of hcn and c2h2 in combustion environment using tdlas. *Processes*, 9, 11 2021. ISSN 22279717. doi: 10.3390/pr9112033.

[49] Shruti Ghanekar, Gavin P. Horn, Richard M. Kesler, Rajavasanth Rajasegar, Jihyung Yoo, and Tonghun Lee. Quantification of elevated hydrogen cyanide (hcn) concentration typical in a residential fire environment using mid-ir tunable diode laser. *Applied Spectroscopy*, 77:382–392, 4 2023. ISSN 19433530. doi: 10.1177/00037028231152498.

[50] Gregory B. Rieker, Jay B. Jeffries, and Ronald K. Hanson. Calibration-free Wavelength-modulation Spectroscopy for Measurements of Gas Temperature and Concentration in Harsh Environments. *Applied Optics*, 48(29):5546–5560, 10 2009. doi: 10.1364/AO.48.005546.

[51] James G. Quintiere. *Fundamentals of Fire Phenomena*. John Wiley & Sons, Ltd, 2006. ISBN 9780470091159.

[52] Dougal Drysdale. *An Introduction to Fire Dynamics*. John Wiley & Sons, Ltd, 2011. ISBN 9781119975465.

[53] Kevin McGrattan, Simo Hostikka, Jason Floyd, Randall McDermott, Marcos Vanella, Eric Mueller, and Chandan Paul. Fire dynamics simulator user's guide, sixth edition. Technical report, NIST Special Publication 1019, National Institute of Standards and Technology, Gaithersburg, MD, 2025.

[54] Richard D. Peacock, Paul A. Reneke, and Glenn P. Forney. Cfast-consolidated model of fire growth and smoke transport (version 7), volume 2: User's guide. Technical report, NIST Technical Note 1889v2, National Institute of Standards and Technology, Gaithersburg, MD, 2025.

[55] D.A. Purser. 19 - Toxic Hazard Calculation Models for use with Fire Effluent Data. In Anna Stec and Richard Hull, editors, *Fire Toxicity*, pages 619–636. Woodhead Publishing, 2010. doi: 10.1533/9781845698072.6.620.

[56] David A Purser and Jamie L McAllister. Assessment of hazards to occupants from smoke, toxic gases, and heat. In Morgan J. Hurley, editor, *SFPE Handbook of Fire Protection Engineering*, volume 2, pages 2308–2428. Springer, New York, 5 edition, 2016. doi: 10.1007/978-1-4939-2565-0.

[57] Subcommittee on Acute Exposure Guideline Levels and Committee on Toxicology and Board on Environmental Studies and Toxicology. *Benzene (CAS Reg. No 71-43-3: Interim Acute Exposure Guideline Levels*. National Academies Press, 2009.

[58] John R. Taylor. *An Introduction to Error Analysis: The Study of Uncertainties in Physical Measurements*. University Science Books, 2 edition, 1997.